Journal of Materials Chemistry A

ROYAL SOCIETY OF CHEMISTRY

PAPER

View Article Online
View Journal | View Issue



Cite this: J. Mater. Chem. A, 2021, 9, 22025

# Radiation-grafted anion-exchange membranes for reverse electrodialysis: a comparison of *N,N,N′,N′*-tetramethylhexane-1,6-diamine crosslinking (amination stage) and divinylbenzene crosslinking (grafting stage)†

Rachida Bance-Soualhi, *[a] Mehdi Choolaei,[ab] Siân A. Franklin,[a] Terry R. Willson,[a] Judy Lee,[b] Daniel K. Whelligan,[a] C. Crean[a] and John R. Varcoe *[a]

Radiation-grafted anion-exchange membranes (RG-AEM) are being developed to evaluate a range of chemistries that have relevance to a variety of electrochemical applications including reverse electrodialysis (RED) salinity gradient power. RG-AEMs are typically fabricated using an electron-beam activated (peroxidated) polymer substrate film. These activated films are first grafted with a monomer, such as vinylbenzyl chloride (VBC) and then reacted with a variety of tertiary amines to yield the desired RG-AEMs. The amination process forms covalently bound quaternary ammonium (QA) head-groups that allow the RG-AEMs to conduct anions such as $Cl^-$. RG-AEMs are of interest as they exhibit high conductivities (100 mS $cm^{-1}$ at elevated temperatures when containing $Cl^-$ anions). However, the current generation of RG-AEMs have two main Achilles' heels: (1) they exhibit low permselectivities; and (2) they exhibit a high degree of swelling in water. Introducing covalent crosslinking into ion-exchange membranes is a well-known strategy to overcome these issues but it often comes with a price – a significantly lowered conductivity (raised *in situ* resistance). Therefore, the level of crosslinking must be carefully optimised. RG-AEMs can be primarily crosslinked using two methods: (1) introduction of a divinyl monomer into the monomer mixture used during grafting; or (2) introduction of a diamine agent into the amination process. This study looks into both methods where either divinylbenzene (DVB) is added into the grafting mixture or *N,N,N′,N′*-tetramethylhexane-1,6-diamine (TMHDA) is added into the amination mixture. We show that on the balance of two application-relevant properties (resistances in aqueous NaCl (0.5 mol $dm^{-3}$) solution and permselectivity), the diamine crosslinking method is the most effective for RG-AEMs being used in RED cells.

Received 18th June 2021
Accepted 8th September 2021

DOI: 10.1039/d1ta05166k

rsc.li/materials-a



## Background and context

Anion-exchange membranes (AEM) are being developed for use as a component in a wide variety of electrochemical technologies[1] such as: fuel cells,[2] electrolysers for green hydrogen generation,[3] electrolysers for $CO_2$ reduction to high value chemicals,[4] redox flow batteries,[5] reverse electrodialysis (RED, a salinity gradient power technology),[6] and electrodialysis for acid recovery[7] and electro-desalination.[8] A class of AEM which exhibits notably high conductivities are radiation-grafted anion-exchange membranes (RG-AEM).[9] However, non-crosslinked, radiation-grafted-type ion-exchange membranes (IEM) generally exhibit undesirably high water uptakes and swelling between the hydrated and dehydrated states,[10] as well as having low permselectivitites[11] (a high permselectivity is important for IEMs targeted for use in RED cells).

The introduction of crosslinking into IEMs can improve permselectivities as well as lower water uptake and swelling.[11–13] However, crosslinking can lower ionic conductivities[11,14–16] so the level of crosslinking needs to be carefully controlled to achieve an optimal balance between properties (*e.g.* improved permselectivities with minimal increases in resistance).[13,17]

RG-AEMs are typically made by treating a polymer film, such as poly(ethylene-*co*-tetrafluoroethylene) (ETFE)[10,18] or non-fluorinated polyethylenes,[19] with high energy radiation (often γ-rays or electron-beams) in air, which peroxidates the films

[a]Department of Chemistry, University of Surrey, Guildford, GU2 7XH UK. E-mail: r.bance-soualhi@surrey.ac.uk; j.varcoe@surrey.ac.uk

[b]Department of Chemical and Process Engineering, University of Surrey, Guildford, GU2 7XH UK

† Electronic supplementary information (ESI) available: Data on a range of ETFE-based radiation-grafted anion-exchange membranes (RG-AEM) made using different diamines to show that *N,N,N′,N′*-tetramethylhexane-1,6-diamine (TMHDA) led to high permselectivity, crosslinked RG-AEMs. A selection of raw data is also available (CC-BY) at 10.6084/m9.figshare.14686875. See DOI: 10.1039/d1ta05166k

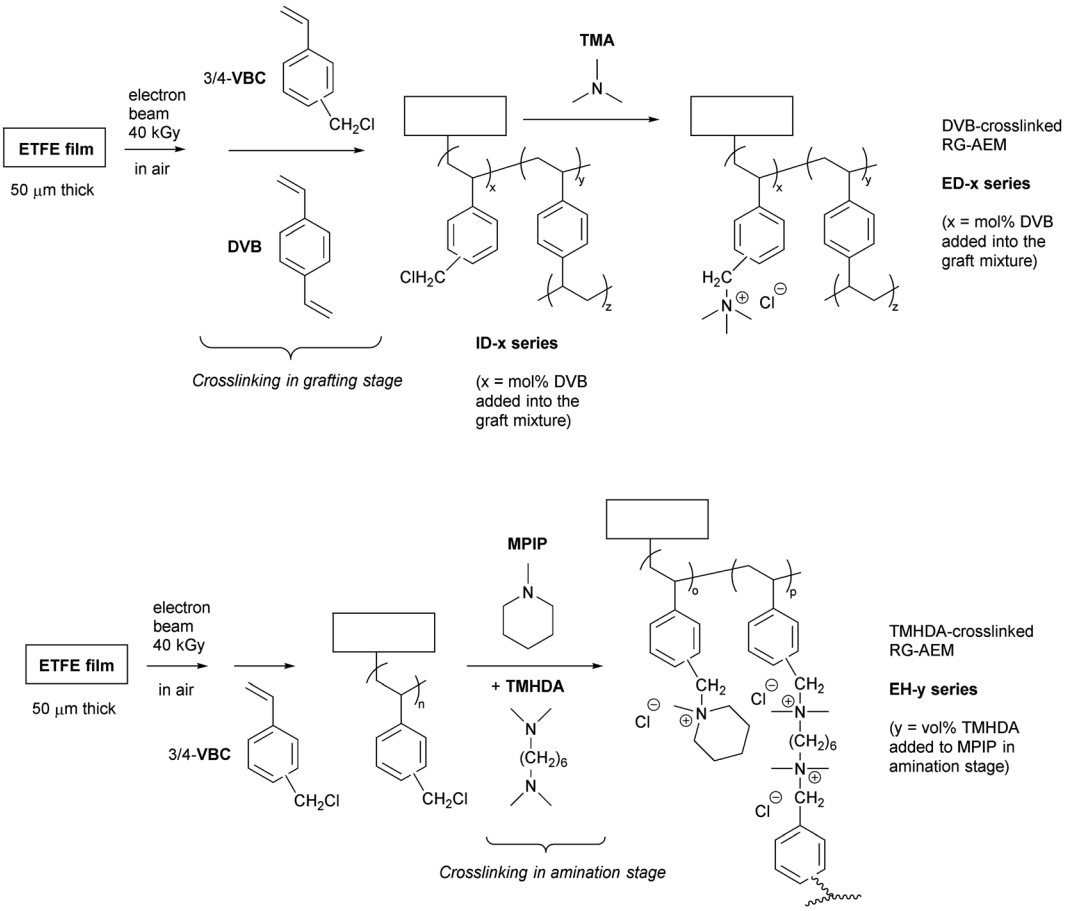


Scheme 1 An outline of the two series of crosslinked radiation-grafted anion-exchange membranes (RG-AEM, $Cl^-$ forms) studied: ED-*x* series involved divinylbenzene (DVB) crosslinking in the grafting stage and the EH-*y* series involved crosslinking in the amination stage using *N*,*N*,*N*′,*N*′-tetramethylhexane-1,6-diamine (TMHDA).

and turns them into free-radical initiators. Vinyl monomers, such as vinylbenzyl chloride (VBC), can then be co-grafted into these radiation-activated films. There is normally a final amination step (*e.g.* treatment of the poly(VBC)-grafted films with a monoamine such as trimethylamine), which converts the non-ionic poly(VBC)-grafted films into RG-AEMs containing covalently-bound quaternary ammonium (QA) groups ($-N^+R_3$). QA groups allow the conduction of anions such as $Cl^-$, $HCO_3^-$, and $OH^-$. There are two synthetic stages where crosslinking can be introduced into the RG-AEMs (Scheme 1): (1) in the grafting stage with the addition of divinyl monomers alongside the main monomer (*e.g.* VBC);[11] (2) in the amination step by addition of a diamine alongside the monoamine.[16]

A UK research project involving our group is to develop RG-AEM chemistries tailored for RED. So far, polymer films have been radiation-grafted with VBC and then aminated with a variety of aliphatic monoamines such as trimethylamine (TMA) and *N*-methylpiperidine (MPIP) as well as aromatic amines such as pyridine. It has been observed that ETFE-based RG-AEMs have a better balance of RED-relevant properties (*e.g.* area resistance *vs.* permselectivity) compared to polyethylene-based RG-AEMs (this is in contrast to RG-AEMs targeted at fuel cells where polyethylene types have better properties).[19]

## Aim and scope of the study

The aim of this study was to elucidate the best synthetic stage in which to introduce crosslinking (grafting or amination stage, Scheme 1) to produce RG-AEMs with a desirable balance of application-relevant properties. To keep this study manageable, we focused on the following:

(a) VBC was radiation-grafted onto 50 μm thick ETFE films;

(b) For crosslinking in the grafting stage, divinylbenzene (DVB) was added into the grafting mixture along with VBC;

(c) For crosslinking in the amination stage, *N*,*N*,*N*′,*N*′-tetramethylhexane-1,6-diamine (TMHDA) was added into the amination mixture containing the monoamine;

(d) To elucidate the best crosslinking method for RED-tailored RG-AEMs, the study focused on the balance between area resistance ($r/\Omega\ cm^2$) and permselectivity ($\alpha$ %).

DVB and TMHDA were selected for this study as they are commercially available reagents that can be purchased in bulk quantities and have been used to crosslink a wide variety of IEMs.[11,16,20,21] As can be seen with the data presented in the ESI† involving ETFE-based RG-AEMs made with a selection of commercially available diamines, TMHDA showed the most promise (on a permselectivity evaluation basis).

 

We initially used TMA as the monoamine amination agent for the DVB-crosslinked series of RG-AEM as this is a common amine used for such purposes. However, when we progressed to the TMHDA-crosslinked series of RG-AEM, TMA could not be used. This is because heat is required to get TMHDA to react with the poly(VBC) in the grafted membranes and TMA (a gas at room temperature and pressure) is normally used in the form of an aqueous solution. *Aqueous TMA solutions should not be heated*: in open vessels the TMA evaporates before amination takes place, while heating in closed glass vessels is dangerous due to a rapid increase in pressure and possible explosion (to keep amination procedures simple for future scale-up, we chose to avoid use of high-pressure autoclaves). Hence, the higher boiling point (>100 °C) amine MPIP[10] was used as the monoamine with TMHDA crosslinker because mixtures of these two high boiling point liquid amines can be safely heated together. As discussed later, this additional variable (using TMA as the monoamine when crosslinking during grafting and MPIP as the monoamine when crosslinking during amination) did not affect the reliability of our conclusions. A further advantage of this switch to MPIP is that it facilitates Raman characterisation of the TMHDA-crosslinked RG-AEMs (as diagnostic absorption bands for TMHDA- and TMA-based QA groups occur at overlapping Raman shifts).

## Materials and methods

### Chemicals and materials

Commercial Nowoflon ET-6235Z ETFE film of 50 μm thickness was supplied by Nowofol Kunstoffprodukte GmbH (Germany) and used as the precursor material for the preparation of all the RG-AEMs membranes in this study. Vinylbenzyl chloride monomer (VBC, 97% purity, mixture of *meta*- and *para*-isomers, initial inhibitor concentrations on purchase: 50–100 ppm 4-*tert*-butylcatechol and 700–1100 ppm nitromethane) and divinylbenzene crosslinker (DVB, technical grade, 80%, mixture of *meta*- and *para*-isomers, initial inhibitor concentrations on purchase: 1000 ppm 4-*tert*-butylcatechol) were purchased from Sigma-Aldrich (now Merck) and used without any further purification or removal of inhibitors. 1-Octyl-2-pyrrolidone dispersant, aqueous trimethylamine solution (TMA, 45 wt%), *N*-methylpiperidine (MPIP, 99%) and *N*,*N*,*N*′,*N*′-tetramethylhexane-1,6-diamine (TMHDA, 99%) were also purchased from Sigma-Aldrich. Standardised analytical aqueous solutions of $AgNO_3$ (0.0200 ± 0.0006 mol $dm^{-3}$), aqueous KOH (0.1000 ± 0.0001 mol $dm^{-3}$) and aqueous $HNO_3$ (2.0 mol $dm^{-3}$) were supplied by Fluka. All other chemicals, including analytical grade NaCl (BioXtra, ≥99.5%), $NaNO_3$(s) and HCl (certified ACS Plus, 37%, used to prepare the aqueous HCl solution) were used as received. Ultrapure water (UPW, resistivity = 18.2 MΩ cm) was used throughout this study. Type-10 AEM and Type 10 cation-exchange membrane (CEM) were kindly supplied by Fujifilm Manufacturing Europe.

### RG-AEM synthesis step 1: electron-beam irradiation of ETFE

A summary of the preparation of the RG-AEMs used in this study is shown in Scheme 1.[18] For the pre-irradiation (peroxidation) step, the ETFE films were irradiated in air to a total absorbed dose of 40 kGy (±10%) *via* cumulative 10 kGy passes on a commercial 4.5 MeV electron-beam (Synergy Health Sterilisation UK Ltd., South Marston site). After irradiation, the irradiated films were stored in dry ice for transport back to the University of Surrey, where they were then stored in a freezer at −40 °C until required for the grafting reaction.

### RG-AEM synthesis step 2: grafting

The pre-irradiated ETFE films (15 × 15 cm lateral dimensions) were immersed in aqueous mixtures containing VBC (5 vol%) and dispersant (1 vol%), both with and without addition of DVB (0–10 mol% in relation to the VBC). The grafting mixtures were then purged by bubbling $N_2$ for 2 h at ambient temperature before the glass vessels were sealed and heated at 70 °C for 24 h. The resulting white, translucent grafted membranes (ID-*x* series where *x* = mol% DVB added) were removed from the grafting mixture and thoroughly washed with toluene before being dried in a vacuum oven at 70 °C.

### RG-AEM synthesis step 3: amination

**ED-*x* series of RG-AEM.** The non-crosslinked and DVB-crosslinked grafted films were aminated with TMA as follows. The grafted films were submerged in the aqueous TMA at ambient temperature for 24 h. The resulting RG-AEMs (designated ED-*x*, where *x* = mol% DVB added to the grafting mixture in relation to the VBC) were then washed with UPW before being heated in water for 8 h at 70 °C.

**EH-*y* series of RG-AEM.** Non-crosslinked grafted films (ID-0) were aminated with MPIP and TMHDA as follows. The grafted film was submerged in a solvent-free mixture of MPIP and TMHDA and heated at 80 °C for 24 h. The resulting RG-AEMs (designated EH-*y*, where *y* = vol% TMHDA added to the liquid MPIP to form the amination mixture) were then washed with UPW before being heated in water for 8 h at 70 °C. Note the highly crosslinked EH-100 (TMHDA-only) was so brittle it would break into pieces on handling.

### RG-AEM synthesis step 4: ion-exchange to $Cl^-$ form

The following procedures were only conducted using polypropylene vessels (to avoid glass-based ion contamination). All RG-AEMs were soaked in excess aqueous NaCl (1.0 mol $dm^{-3}$) solution for 12 h (with several changes of solution during this period, to ensure only $Cl^-$ anions were present). The final $Cl^-$ form RG-AEMs were obtained after thorough washing in UPW (over 16 h with at least 5 changes in UPW to removal all excess counter- and co-ions) before being stored in UPW until required for characterisation or testing.

### Pre-treatment of the commercial Fujifilm IEMs

Before use in benchmarking measurements, the Fujifilm IEMs were immersed in excess aqueous NaCl (1 mol $dm^{-3}$) solution for 48 h (with two changes of solution in this time) to exchange them to either the $Na^+$ form for the CEM or the $Cl^-$ form for the AEM. Subsequently, the IEMs were washed multiple times with

UPW (to remove all excess co- and counter-ions). The prepared commercial IEMs membranes were stored in UPW until required.

### Raman spectroscopy

Raman spectra of the ETFE precursor, the grafted films and the final RG-AEMs were recorded with a Renishaw InVia Reflex Raman Microscope (Renishaw, UK) using 785 nm laser excitation (near-IR line laser, pin in to form a spot, 100% laser power setting) and a 50XL objective. Spectra were recorded with accumulation over 4 scans and 1 s exposures. Spectra were recorded on 5 random spots on each side of a sample of each RG-AEM, which were then baseline corrected, normalised to the intensity of an ETFE-derived band (see figure captions) and averaged into 1 spectrum per RG-AEM. Spectral deconvolution (band decomposition) was conducted using OriginLab Origin software.

### Gravimetric water uptakes (WU) and water contents ($\lambda_{water}$)

Excess surface water on samples of the fully hydrated IEMs (as prepared above) were removed by dabbing with filter paper before immediately weighing to give the hydrated sample masses ($m_h$/g). The samples were then dried in a vacuum oven at 50 °C for 15 h before the dry masses ($m_d$/g) were recorded. All measurements were repeated with $n = 3$ samples of each RG-AEM. The gravimetric WUs were calculated as follows:

$$\mathrm{WU}(\%) = 100 \times \frac{m_h - m_d}{m_d} \quad (1)$$

Water contents ($\lambda_{water}$, the number of absorbed water molecules per QA group or monovalent counter anion) were calculated as follows:

$$\lambda_{water} = \frac{(\mathrm{WU}/100)}{\mathrm{IEC} \times \mathrm{MW}(H_2O)} \quad (2)$$

where the IEC ($\mathrm{mol_{QA}\ g_{IEM(dry)}^{-1}}$) is the ion-exchange capacity of the sample (determined as described below) and $\mathrm{MW}(H_2O) = 18.0153\ \mathrm{g\ mol^{-1}}$.

### Ion-exchange capacities (IEC)

The IECs of the RG-AEMs, which is the number of fixed charges per unit mass of the membrane, was measured using the $Cl^-$ precipitation titration method.[10,18] The IECs were determined using the dried AEM samples (in $Cl^-$ form) recovered from WU measurements above. These RG-AEM samples were soaked in aqueous $NaNO_3$ (20.0 $cm^3$, 2.4 mol $dm^{-3}$) solution for at least

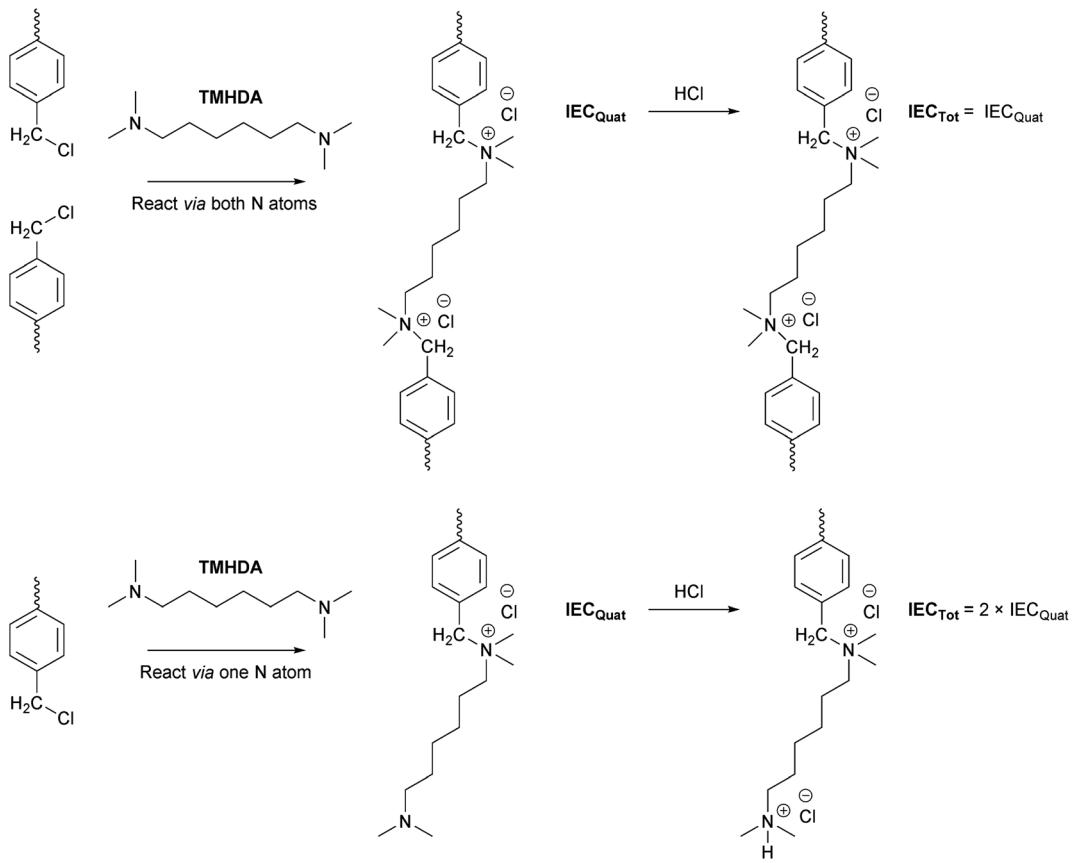


Scheme 2 An overview of the reaction of the grafted poly(VBC) chains with TMHDA in both a crosslinking (reaction of both N atoms) and a non-crosslinking (reaction of a single N atom) mode. A subsequent reaction with HCl (to quaternise any remaining tertiary amines) allows for the titrimetric-based determination of the ratio of crosslinking to non-crosslinking reaction of TMHDA (by comparing the resulting $IEC_{Quat}$ and $IEC_{Tot}$ values).

6 h before the solutions were acidified with $HNO_3$ (2 $cm^3$, 2 mol $dm^{-3}$). The solutions (still containing the RG-AEM samples) were then titrated with aqueous $AgNO_3$ (0.0200 ± 0.0006 mol $dm^{-3}$) solution using a Metrohm 848 Titrino plus Autotitrator equipped with an Ag-Titrode combined electrode. The IEC (mmol $g^{-1}$) of each sample was calculated from the endpoint (EP/$cm^3$):

$$\mathrm{IEC} = \frac{\mathrm{EP} \times 0.02}{m_\mathrm{d}} \quad (3)$$

where $m_d$ is the dry mass (g) of the RG-AEM sample in the $Cl^-$ form.

The TMHDA-crosslinked RG-AEMs (EH-5 to EH-100) require a more detailed titration protocol in order to detect both the amounts of QA and tertiary amine (TA) groups (see Scheme 2). For these, the IECs determined as described above are labelled $IEC_{Quat}$. The total IECs ($IEC_{Tot}$), which is the amount of QA + TA groups per unit mass of dry RG-AEM ($Cl^-$ form), were determined as follows: weighed, dried RG-AEM($Cl^-$) samples were treated with aqueous HCl (1 mol $dm^{-3}$) for 12 h prior to being thoroughly washed with UPW (to remove all excess co- and counter-ions), immersed in aqueous $NaNO_3$ for at least 6 h, and titrated as detailed above.

The IEC of the Fujifilm CEM was determined using the titration protocol detailed in ref. 11. As this procedure is subsidiary to the focus of this study, this procedure will not be repeated here.

### Thicknesses and thickness swelling (TPS)

When samples of each RG-AEM were being weighed for the WU experiments described above, their thicknesses were also recorded (giving $t_h$ and $t_d$, the hydrated and dehydrated thicknesses, respectively). This allowed for the calculation of the thickness (through-plane) swelling (TPS):

$$\mathrm{TPS}(\%) = 100 \times \frac{t_\mathrm{h} - t_\mathrm{d}}{t_\mathrm{d}} \quad (4)$$

### In-plane $Cl^-$ conductivities (RG-AEMs in water)

The in-plane $Cl^-$ conductivities of the fully hydrated RG-AEMs (and $Na^+$ conductivity of the Fujifilm CEM) were determined using electrochemical impedance spectroscopy (EIS) and a four-point BekkTech (BT-112) conductivity test cell (supplied by Alvatek, UK). Hydrated samples of each RG-AEM ($Cl^-$ form) and Fujifilm CEM ($Na^+$ form) were cut into strips (1 cm × 3 cm) and individually mounted in the conductivity cell. The cell was then submerged in UPW at 25 °C. The resistance ($R/\Omega$) of each IEM sample was measured using a Solartron 1260/1287 instrument combination controlled by ZPlot (Scribner Associates, USA). The EIS data were recorded using a.c. voltage perturbations of 10 $mV_{rms}$ amplitude over the frequency range 0.5 Hz to 100 kHz (open circuit with no applied d.c. bias). Ionic resistance values were extracted from the Nyquist plots as the low frequency $x$-axis intercept (as per the cell instructions). The conductivity ($\sigma$/mS $cm^{-1}$) of each sample was then calculated:

$$\sigma = \frac{d}{R \times w \times t_\mathrm{h}} \quad (5)$$

where $d$ is the distance between two electrodes (0.425 cm), $R$ is the measured resistance (Ω) and $w$ and $t$ are the width and thickness of the fully hydrated IEM sample, respectively.

### Through-plane area resistances in aqueous NaCl (0.5 mol $dm^{-3}$)

The through-plane resistances of the IEMs in aqueous NaCl (0.5 mol $dm^{-3}$) solutions were recorded using a Scribner H-Cell (a 4-electrode 2-compartment cell supplied by Scribner Associates Inc., USA). Two Pt wire electrodes were used as the working and counter electrodes (WE, CE – forming the current circuit), along with two Ag/AgCl (3 mol $dm^{-3}$ KCl) reference electrodes (RE) (fitted into Luggin capillaries that were positioned on either side of the IEM sample under test with 2 mm distances between the capillary tip and the IEM surface). The effective area ($A$) of the IEM under investigation was 4.91 $cm^2$. Prior to measurement, each IEM sample was equilibrated in aqueous NaCl solution (0.5 mol $dm^{-3}$) for at least 24 h. The electrical resistance was measured at room temperature using a Solartron 1287 potentiostat controlled by Scribner CorrWare software. A constant 10 mV $s^{-1}$ d.c. potential sweep was applied between the two RE over the range −0.10 and +0.10 V. The resistance was taken as the slope of the recorded potential *vs.* current plot. Two runs were performed both with and without the IEM test sample. The area specific resistance of the IEM ($r/\Omega$ $cm^2$) was calculated by subtracting the resistance measured without membrane (solution resistance, $R_S$) from the resistance measured with membrane ($R_{M+S}$):

$$r = A \times (R_{\mathrm{M+S}} - R_\mathrm{s}) \quad (6)$$

All measurements were repeated with $n = 3$ samples of each IEM.

### Permselectivities ($\alpha$)

Permselectivity describes the degree to which an IEM excludes co-ions and was determined in this study using a static membrane potential measurement.[22] A home-made cell made of Plexiglass was used, which consisted of two chambers separated by the IEM sample under test (effective area of 25 $cm^2$). The cell chambers were subsequently filled with aqueous NaCl solutions of differential concentrations (0.1 mol $dm^{-3}$ and 0.5 mol $dm^{-3}$). The aqueous NaCl solutions were continuously circulated (single pass) using two peristaltic pumps (Cole-Parmer, Masterflex L/S Digital drive, USA). Before permselectivity determinations, each IEM sample under test was conditioned overnight in aqueous NaCl (0.1 mol $dm^{-3}$) solution. Two double junction Ag/AgCl REs (Metrohm) were placed in the solution on either side of the IEM under test. The electrical potential difference across membrane ($E$) was recorded using an Autolab PGSTAT302N potentiostat (Metrohm). The experimental membrane potential ($E_M$) was then obtained by subtracting the offset potential ($E_{offset}$) from $E$. $E_{offset}$ was measured as the potential difference between the two REs (with the same spacing) immersed in the same cell without an IEM that contained aqueous NaCl (0.5 mol $dm^{-3}$) solution. The

permselectivity ($\alpha$) was then calculated from the ratio of the experimentally determined $E_M$ to the theoretical potential ($E_T$, the membrane potential for a 100% permselective IEM calculated from the Nernst equation, taken as 37.9 mV in this study):[22,23]

$$\alpha(\%) = 100 \times \frac{E - E_{offset}}{E_T} \quad (7)$$

All measurements were repeated with $n = 3$ samples of each IEM.

## Results and discussion

### ETFE-based RG-AEMs with DVB-based crosslinking (ED-*x* series)

**Raman spectroscopic confirmation of grafting, crosslinking and amination.** Fig. 1 presents the Raman spectra of the pre-aminated VBC- and DVB-co-grafted membranes (ID-0 to ID-10). These spectra confirm grafting of the poly(VBC) chains onto the ETFE polymer chains, as previously reported in detail, with the superposition of the spectrum for poly(VBC) homopolymer and ETFE homopolymer.[10,18] Key absorption bands to highlight:

- 1268 $cm^{-1}$ band diagnostic of $-CH_2Cl$ groups;
- 1612 $cm^{-1}$ aromatic ring quadrant mode that is diagnostic of the presence of the benzene rings in the poly(VBC) grafted chains;
- 1002 $cm^{-1}$ band that is diagnostic of the breathing mode of *meta*-disubstituted benzene rings from the grafting of the *meta*-VBC isomer in the commercially supplied *meta*- and *para*-isomer mixture of VBC monomer (this band is not present for *para*-disubstituted benzene rings).

It was observed that the integrated area of the 1612 $cm^{-1}$ band was 8% higher for ID-1 than it was for ID-0 (when normalised against the intensity of the deconvoluted 946 $cm^{-1}$ ETFE-derived band), which suggests that the addition of 1 mol% DVB into the grafting mixture boosted the amount of VBC that grafted. This phenomenon has been reported before,[15,24] where the presence of a monomer that undergoes facile radical chain-growth polymerisation (DVB in this case) can boost the grafting of a monomer that has slower kinetics for radical chain-growth (VBC in this case). This phenomenon will be discussed further when IEC values are compared below.

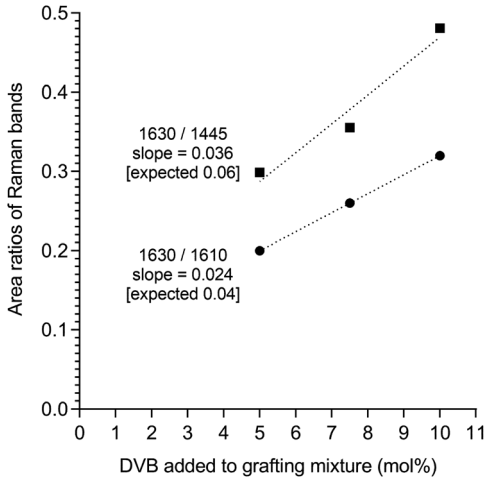


Fig. 2 The variation in the ratios of the integrated areas of key Raman bands for the pre-aminated grafted membranes containing the higher DVB crosslinking contents (ID-5, ID-7.5 and ID-10). The 1630 $cm^{-1}$ band is assigned to the benzene ring of the DVB co-grafts, the 1610 $cm^{-1}$ band is assigned to the benzene rings of the VBC grafts and the 1445 $cm^{-1}$ band is the $CH_2$ scissor mode for ETFE.

For the DVB + VBC co-grafted membranes with a significant amount of DVB added into the grafting mixture (ID-2.5 to ID-10) an additional band was observed at *ca.* 1630 $cm^{-1}$. This band is due to the presence of the grafted DVB crosslinker, as also observed for DVB- and styrene-co-grafted membranes previously used to produce radiation-grafted cation-exchange membranes (RG-CEM).[11] Fig. 1 shows that an increase in the amount of DVB added to the grafted mixture (ID-2.5 to ID-10) led to an increase in the intensity of the 1630 $cm^{-1}$ band,

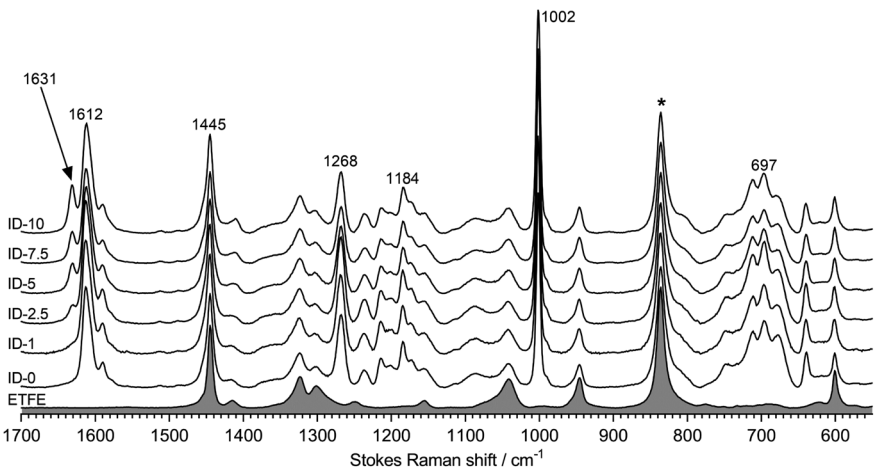


Fig. 1 The Raman spectra of the pre-aminated grafted membranes (ID-0 to ID-10) and ETFE precursor film (shaded). The spectra were recorded with a laser $\lambda = 785$ nm and a 50× objective. *Spectral intensities normalised to this band.

 

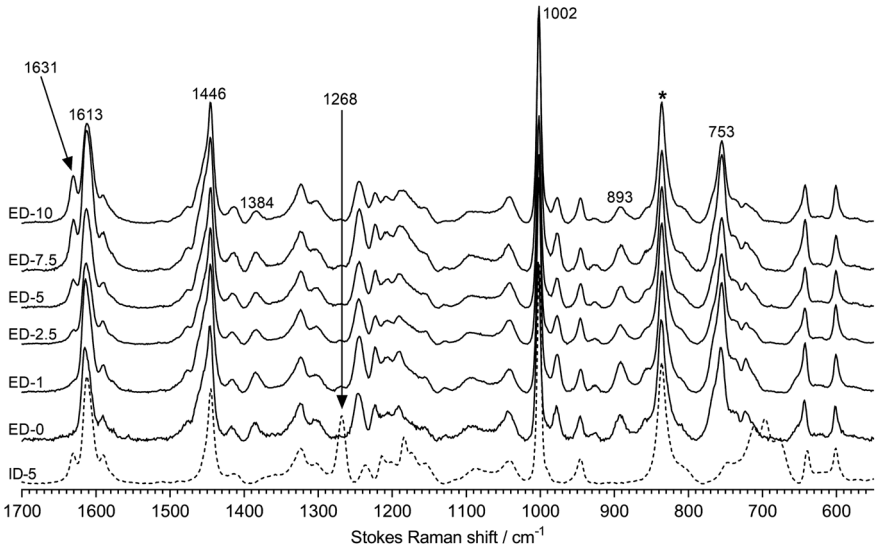


Fig. 3 The Raman spectra of the RG-AEMs (ED-0 to ED-10, TMA, $Cl^-$ forms) and the pre-aminated grafted membrane ID-5 (dashed). The spectra were recorded with a laser $\lambda = 785$ nm and a 50× objective. *Spectral intensities normalised to this band.

which indicates an increasing amount of co-grafted DVB crosslinker in the RG-AEMs. This was analysed in more detail for ID-5, ID-7.5 and ID-10, where the integrated areas of the deconvoluted 1630 $cm^{-1}$ band was normalised to the integrated areas of both the deconvoluted poly(VBC)-derived 1610 $cm^{-1}$ band and the deconvoluted ETFE $CH_2$ scissor mode band at 1445 $cm^{-1}$ (Fig. 2). This shows an increased amount of DVB in the grafting mixture led to an increase in the amount of co-grafted DVB but doubling the amount of DVB in the grafting mixture did not result in double the amount of co-grafted DVB. This highlights the complexity involved when monomers mixtures are used to produce radiation-grafted membranes.

Fig. 3 gives the Raman spectra for the final RG-AEMs in the $Cl^-$ forms (ED-0 to ED-10). These spectra confirm amination with minimal residual intensity of the 1268 $cm^{-1}$ band (an intense band that is present in the pre-aminated grafted membranes). The appearance of a diagnostic band at 753 $cm^{-1}$ confirms the presence of benzyltrimethylammonium groups.[10,18]

**Ion-exchange capacities, water uptakes and swelling.** Keystone properties for the ED-*x* series of RG-AEMs are summarised in Table 1 (alongside data collected on Fujifilm commercial Type-10 IEMs). The IEC of ED-1 was 5% higher compared to the RG-AEM made with only VBC (no DVB) in the grafting mixture (ED-0) (Fig. 4). This is consistent with the

Table 1 Key properties for the TMA- and ETFE-based RG-AEMs synthesised using divinylbenzylene (DVB) as crosslinking agent (designated ED-*x* where *x* = mol% DVB added into the grafting mixture), where errors are sample standard deviations from $n = 3$ replicates unless otherwise stated. The properties of the Fujifilm AEM and CEM are also included for comparison purposes. Properties are for the $Cl^-$ forms unless otherwise stated

| AEM (in $Cl^-$ form) | $t_{hydrated}$/ μm[a] | IEC/ mmol $g^{-1}$ | WU (wt%) | $\lambda_{water}$[b] | Conductivity, $\sigma$/mS $cm^{-1}$[c] | Area resistance, $r^d$/Ω $cm^2$ | Permselectivity $\alpha^e$ (%) |
|---|---|---|---|---|---|---|---|
| Fujifilm AEM type 10 | 127 ± 3 | 2.51 ± 0.07 | 42 ± 3 | 9 ± 1 | 4.8 ± 0.5 | 1.61 ± 0.08 [1.7][f] | 93.5 ± 1.3 [95][f] |
| ED-0 | 92 ± 2 | 1.68 ± 0.03 | 49 ± 3 | 16 ± 1 | 14.2 ± 0.1 | 0.52 ± 0.07 | 82.4 ± 0.2 |
| ED-1 | 85 ± 2 | 1.76 ± 0.04 | 48 ± 4 | 15 ± 1 | 15.3 ± 0.9 | 0.49 ± 0.06 | 83.4 ± 1.1 |
| ED-2.5 | 83 ± 2 | 1.72 ± 0.07 | 39 ± 5 | 13 ± 2 | 11.3 ± 1.1 | 0.74 ± 0.07 | 86.9 ± 0.7 |
| ED-5 | 78 ± 2 | 1.51 ± 0.05 | 23 ± 3 | 9 ± 1 | 7.8 ± 0.4 | 1.11 + 0.19 | 85.9 ± 1.3 |
| ED-7.5 | 73 ± 2 | 1.43 ± 0.09 | 18 ± 3 | 7 ± 1 | 5.6 ± 0.3 | 1.64 ± 0.27 | 91.1 ± 1.9 |
| ED-10 | 70 ± 2 | 1.34 ± 0.07 | 15 ± 6 | 7 ± 3 | 4.4 ± 0.2 | 2.31 ± 0.08 | 93.4 ± 1.1 |
| Fujifilm CEM type 10[g] | 132 ± 4 | 2.64 ± 0.01 | 39 ± 5 | 8 ± 1 | 3.8 ± 0.3 | 2.08 ± 0.21 [2.0][f] | 95.1 ± 0.2 [99][f] |

[a] Errors are sample standard deviations from $n = 3$ measurements on each membrane or 2 μm (the minimum visual precision of the micrometer used), whichever is the greatest. [b] Errors are propagated uncertainties (calculated from the errors of input parameters). [c] In-plane conductivities of the $Cl^-$ form AEMs ($Na^+$ form for CEM type 10) in water at 25 °C (with no co-ions or excess counter ions present). [d] Through-plane area resistances in aqueous NaCl (0.5 mol $dm^{-3}$) at room temperature. [e] The errors in room temperature permselectivities are sample standard deviations from $n = 3$ repeat measurements ($n = 2$ for the Fujifilm CEM) but these are smaller than the expected uncertainties of ± 3% (assuming $a$ ± 1 mV error in electrode potential readings). [f] Data in [] are resistance and permselectivity values provided by the manufacturer for comparison purposes. [g] Values for $Na^+$ form (this CEM was studied to provide further experimental validation of resistance and permselectivity measurements and was characterised for IEC and conductivity using the methods described in ref. 11).

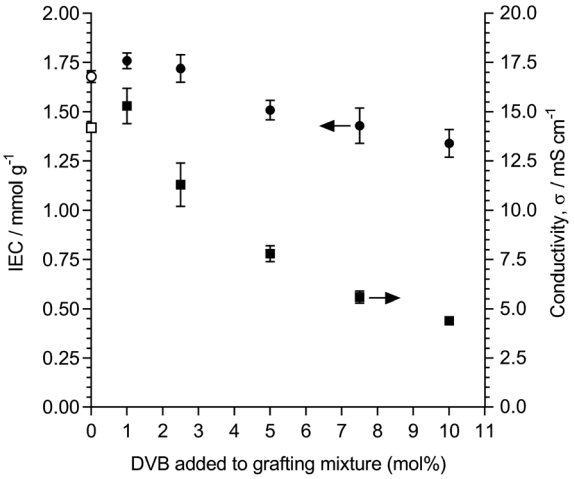


Fig. 4 The variation in IEC (circles) and $Cl^-$ conductivity (squares, in water, in-plane, 25 °C) of the RG-AEMs (TMA) made using increasing DVB in the grafting stage. Error bars are sample standard deviations ($n = 3$).

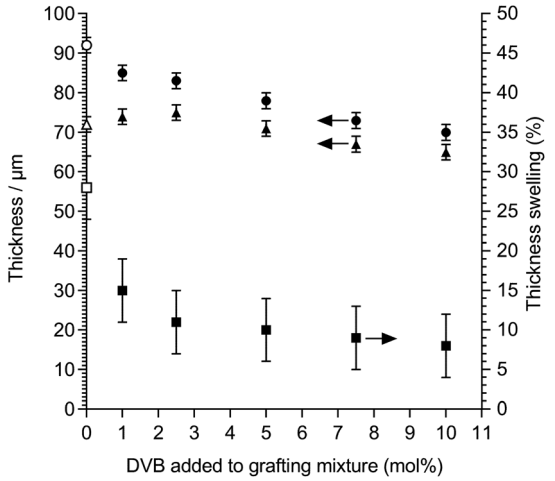


Fig. 6 The variation in hydrated thickness (circles), dry thickness (triangles) and dimensional swelling on hydration in the thickness direction (squares) of the RG-AEM (TMA, $Cl^-$ forms) made using increasing DVB in the grafting stage. Error bars for percentage thickness swelling values are propagated uncertainties calculated from the errors in measured thicknesses ($n = 3$ repeat measurements for each hydration state).

Raman data discussed above and shows that addition of a small amount of DVB to the grafting mixture has a boosting effect on VBC grafting.[14,15,24] This increased amount of grafted poly(VBC) chains leads to a higher IEC when aminated. With further increases in the amount of DVB crosslinker added to the grafting mixture, the IEC of the resulting RG-AEMs decreases (ED-2.5 to ED-10).

A lowered IEC combined with increasing contents of crosslinking should lead to decreased water uptakes and swelling and this was observed. The water contents, expressed either as a gravimetric percentage (WU) or number of water molecules per anion ($\lambda_{water}$), decreased on increasing DVB-crosslinking (Fig. 5). This then manifests itself as a decline in hydrated thickness and thickness swelling (Fig. 6), which was one of the desired outcomes of adding a crosslinker. The reduction in thickness swelling was dramatic when transitioning from non-crosslinked ED-0 to lightly crosslinked (higher IEC) ED-1, after which it starts to plateau out with less dramatic reductions in swelling with higher levels of crosslinking (ED-2 to ED-10). The next question to address is does DVB-crosslinking and reduced water contents lead to a decrease in conductivity?

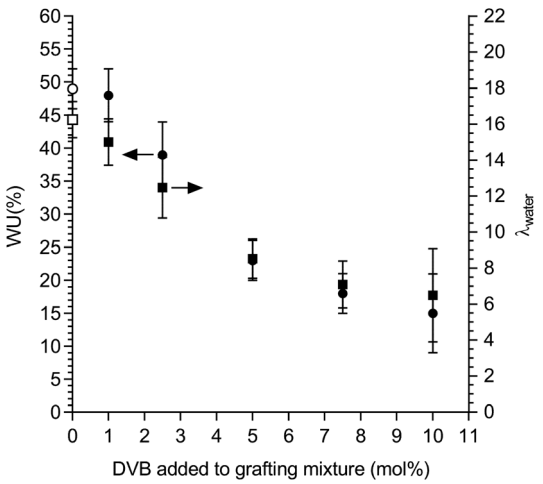


Fig. 5 The variation in gravimetric water uptake (WU, circles) and the number of $H_2O$ molecules per $Cl^-$ anion ($\lambda_{water}$, squares) of the RG-AEMs (TMA, $Cl^-$ forms) made using increasing DVB in the grafting stage. Error bars for WU are sample standard deviations ($n = 3$). Error bars for $\lambda_{water}$ are propagated uncertainties calculated from the errors in measured IEC and WU values.

**Ionic conductivity ($Cl^-$ form in water), area resistance (in contact with aqueous NaCl), and permselectivity.** Fig. 4 shows that the $Cl^-$ anion conductivity tracks the IEC and there is a significant reduction in conductivity on increasing the amount of crosslinking. The drop in conductivity is larger than the drop in IEC as there is also a concomitant decrease in water content. Using DVB as the crosslinking agent does appear to have limitations: achieving a reasonable decrease in swelling results in an undesirably large decrease in conductivity.

However, these in-plane AEM-intrinsic conductivities (pure $Cl^-$ form RG-AEMs in water) are not directly representative of the resistances that are relevant to application in RED. Hence, the through-plane area resistances were also measured when the RG-AEMs were in contact with aqueous NaCl (0.5 mol dm$^{-3}$) solutions at room temperature. These more application-relevant through-plane resistances were compared to the in-plane conductivities (Fig. 7). As expected, as the $Cl^-$ conductivities decrease (with increased crosslinking, ED-1 to ED-10), the area resistances increase.

The nonlinear correlation observed in Fig. 7 relates to the differences in the test conditions used for the in- and through-plane measurements. As has been reported,[25,26] the volume of an ion-exchange polymer tends to decrease with an increase in the concentration of an external salt solution, that it is in contact with, due to osmotic de-swelling. Since the number of

 

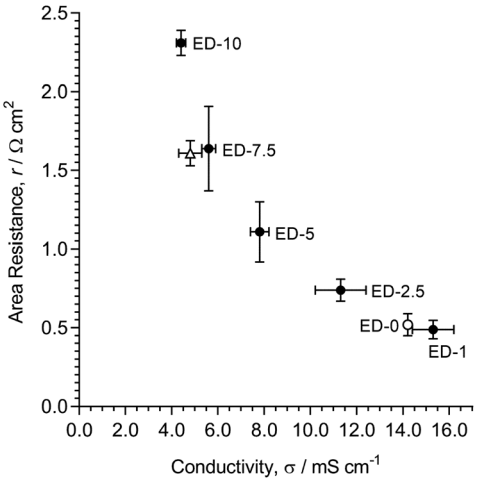


Fig. 7 The relationship between the room temperature (20–25 °C) through-plane area resistances (2-compartment cell containing aqueous NaCl (0.5 mol $dm^{-3}$) solution) and intrinsic $Cl^-$ conductivities (25 °C, in water, in-plane, no co-ions or excess counter-ions) of the RG-AEMs (TMA) made using DVB crosslinker. The triangle datapoint is for the Fujifilm AEM (commercial benchmark).

counter-anions that balance the QA groups in the AEM is constant, a decrease in the swollen membrane volume will increase the charge density of the counter-ions. This increase can retard the mobility of the charge carriers in the membrane and further increase the difference of the ion transport number between the bulk solution (by both co- and counter-ions) and the IEM (by counter-ions due to the Donnan exclusion effect). Generally, this difference in the ion transport number between the bulk solution and the IEM results in a build-up of a diffusion boundary layer at the membrane surface, which impedes charge transfer processes in the system.[27] A reduced AEM volume, especially with increased crosslinking (naturally retarded swelling), with *in situ* contact with aqueous salt solutions (in the through-plane resistance measuring cell) would result in an increased contribution of the diffusion boundary layer resistance to the overall resistance. Thus, the observed nonlinear relationship between the in-plane conductivity and the through-plane resistance, especially with higher levels of crosslinking, is consistent with the observed area resistances reflecting the system, with a contribution of the diffusion boundary layer resistance alongside a change in the resistance from the AEM itself.

As expected, an increasing level of DVB-crosslinking led to an increase in permselectivity ($\alpha$, Table 1). Using DVB crosslinker, quite a high level of crosslinking was required to achieve $\alpha$ values of >90%, which meant the RG-AEMs exhibited undesirably high area resistances.

### ETFE-based RG-AEMs with TMHDA-based crosslinking (EH-*x* series)

**Raman spectroscopic confirmation of amination.** Fig. 8 present the Raman spectra for EH-0 to EH-100. All spectra show no significant evidence of a band at 1268 $cm^{-1}$ indicating that the $-CH_2Cl$ groups in the poly(VBC) chains of the pre-aminated grafted membrane have reacted with the tertiary amines. The spectrum of the non-crosslinked, TMHDA-free EH-0 shows the expected bands for MPIP-based head-groups (*e.g.* at 1360, 1272, 1030, 705 $cm^{-1}$).[10,28] The spectrum for the MPIP-free EH-100 shows some characteristic bands for TMHDA-based QA groups such as the broad band at 757 $cm^{-1}$.

The remaining spectroscopic discussions will focus on the band at 1272 $cm^{-1}$ as this is present for MPIP-based groups but not for TMHDA-based groups. The intensity of the band generally declines from EH-0 to EH-20 (note a similar trend is observed for other MPIP-based bands such as the band at

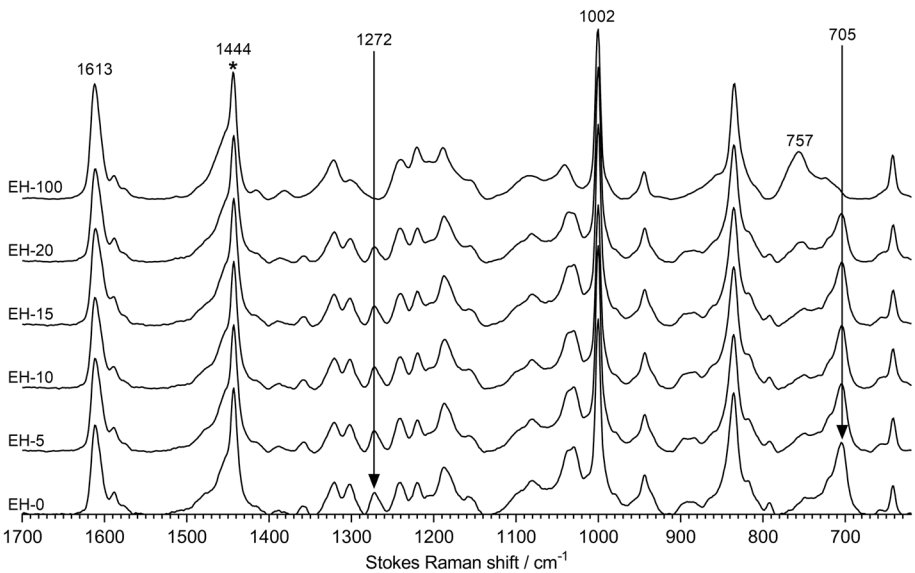


Fig. 8 The Raman spectra of the RG-AEMs (EH-0 to EH-100, aminated with MPIP-TMHDA mixtures, $Cl^-$ forms). The spectra were recorded with a laser $\lambda = 785$ nm and a 50× objective. *Spectral intensities normalised to this band.

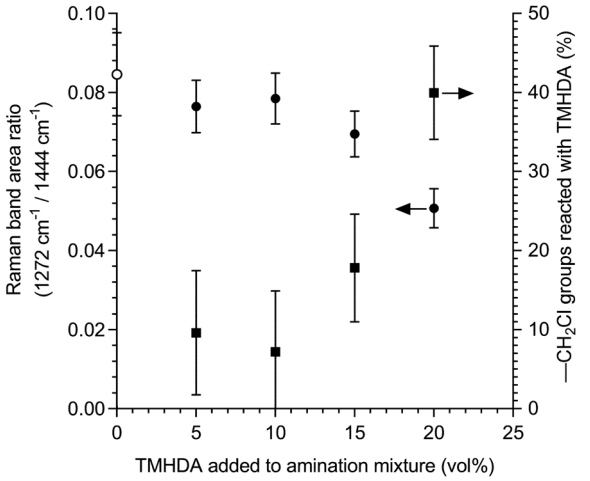


Fig. 9 The left-hand *y*-axis (circle data) gives ratio of the area of the 1272 cm$^{-1}$ band normalised to the area of the 1444 cm$^{-1}$ ($AR_{1272/1444}$) in the spectra of EH-0 to EH-20 (spectra in Fig. 8). The 1272 cm$^{-1}$ is assigned to the MPIP-based head-groups, while the 1444 cm$^{-1}$ band is assigned to the $CH_2$ scissor mode of the ETFE substrate. The error bars for $AR_{1272/1444}$ are sample standard deviations over values extracted from $n = 10$ spectra for each RG-AEM ($n = 5$ spectra per side of each RG-AEM sample). The right-hand *y*-axis (square data) gives the percentage of the $-CH_2Cl$ groups of the pre-aminated grafted membrane that have reacted with the TMHDA crosslinker, which was estimated from the mean $AR_{1272/1444}$ values according to eqn (8).

705 cm$^{-1}$). Hence the area of this band normalised to the area of the ETFE-derived ($CH_2$ scissor mode) band at 1444 cm$^{-1}$ (designated $AR_{1272/1444}$ hereon), which has minimal overlap with other bands in these spectra, should give an indication of the ratio of MPIP- to TMHDA-based reactions with the $-CH_2Cl$ groups (Fig. 9). The MPIP-based head-group content (values for $AR_{1272/1444}$) generally decrease with the use of an increasing amount of TMHDA crosslinker in the amination mixture. The ratio for EH-5 and EH-10 is off trend, but it should be kept in mind that the Raman experiments are only sampling 5 random spots (*ca.* 2 μm in size) on each face of each RG-AEM sample and the precision achievable with such analysis (*i.e.* the error bars in Fig. 9).

This $AR_{1272/1444}$ data can be used to estimate the percentage of the $-CH_2Cl$ groups of the pre-aminated poly(VBC)-grafted membranes reacted with the TMHDA crosslinker, which was calculated (with the assumption of homogeneous poly(VBC) grafting) using:

$$\text{TMHDA reaction}(\%) = 100 \times \left(1 - \frac{AR_{1272/1444}(EH\text{-}y)}{AR_{1272/1444}(\text{EH-0})}\right) \quad (8)$$

where $AR_{1272/1444}$(EH-*y*) is the band area ratio for the RH-AEM made with *y* vol% TMHDA in the amination mixture and $AR_{1272/1444}$(EH-0) is the ratio for the TMHDA-free MPIP-only RG-AEM. As can be seen in Fig. 9 (right-hand *y*-axis data), the TMHDA generally reacts to a greater extent than would be

Table 2 Key properties for the MPIP- and ETFE-based RG-AEMs synthesised using *N*,*N*,*N*′,*N*′-tetramethylhexane-1,6-diamine (TMHDA) as crosslinking agent (designated EH-*y* where *y* = vol% TMHDA added to the MPIP to form the amination mixture), where errors are sample standard deviations from $n = 3$ replicates unless otherwise stated. The properties of the non-crosslinked TMA-based RG-AEM (ED-0 from Table 1) is also included for comparison purposes (alongside the Fujifilm AEM data for completeness). Properties are for the $Cl^-$ forms unless otherwise stated

| AEM (in $Cl^-$ form) | $t_{hydrated}$/μm[a] | $IEC_{Quat}$ {$IEC_{Tot}$}/ mmol g$^{-1}$ ⟨$IEC_{Tot}/IEC_{Quat}$⟩ | WU (% wt.) | $\lambda_{water}$[b] | Conductivity, $\sigma$/mS cm$^{-1}$[c] | Area resistance, $r^d$/Ω cm$^2$ | Permselectivity $\alpha^e$ (%) |
|---|---|---|---|---|---|---|---|
| Fujifilm AEM type 10 | 127 ± 3 | 2.51 ± 0.07 | 42 ± 3 | 9 ± 1 | 4.8 ± 0.5 | 1.61 ± 0.08 [1.7][f] | 93.5 ± 1.3 [95][f] |
| ED-0 | 92 ± 2 | 1.68 ± 0.03 | 49 ± 3 | 16 ± 1 | 14.2 ± 0.1 | 0.52 ± 0.07 | 82.4 ± 0.2 |
| EH-0 | 94 ± 3 | 1.59 ± 0.05 | 56 ± 1 | 20 ± 1 | 12.1 ± 1.1 | 0.49 ± 0.09 | 78.5 ± 1.2 |
| EH-5 | 94 ± 2 | 1.48 ± 0.01 {1.56 ± 0.05} ⟨1.05 ± 0.03⟩[b] | 34 ± 2 | 13 ± 1[g] | 9.2 ± 0.5 | 0.67 ± 0.40 | 88.2 ± 1.0 |
| EH-10 | 91 ± 2 | 1.47 ± 0.03 {1.57 ± 0.02} ⟨1.07 ± 0.03⟩[b] | 32 ± 1 | 12 ± 1[g] | 9.0 ± 0.7 | 0.85 ± 0.13 | 89.5 ± 1.0 |
| EH-15 | 84 ± 2 | 1.41 ± 0.04 {1.44 ± 0.14} ⟨1.02 ± 0.10⟩[b] | 29 ± 2 | 11 ± 1[g] | 7.9 ± 0.8 | 1.07 ± 0.17 | 90.6 ± 0.5 |
| EH-20 | 89 ± 2 | 1.43 ± 0.05 {1.46 ± 0.02} ⟨1.02 ± 0.04⟩[b] | 24 ± 2 | 9 ± 1[g] | 4.6 ± 0.3 | 1.38 ± 0.21 | 91.8 ± 0.7 |
| EH-100 | 83 ± 2 | 1.37 ± 0.06 {1.46 ± 0.03} ⟨1.07 ± 0.05⟩[b] | 20 ± 2 | 8 ± 1[g] | –[h] | –[h] | 94[h] |

[a] Errors are sample standard deviations from $n = 3$ measurements on each membrane or 2 μm (the minimum visual precision of the micrometer used), whichever is the greatest. [b] Errors are propagated uncertainties (calculated from the errors of input parameters). [c] In-plane conductivities of the $Cl^-$ form AEMs in water at 25 °C (with no co-ions or excess counter-ions present). [d] Through-plane area resistances in aqueous NaCl (0.5 mol dm$^{-3}$) at room temperature. [e] The errors in room temperature permselectivities are sample standard deviations from $n = 3$ repeat measurements but these are smaller than the expected uncertainties of ±3% (assuming $a \pm 1$ mV error in electrode potential readings). [f] Data in [] are resistance and permselectivity values provided by the manufacturer for comparison purposes. [g] $\lambda_{water}$ calculated using $IEC_{Quat}$ values. [h] AEM was too brittle to retain integrity in the measurement cells (1 measurement of permselectivity was achieved).

 

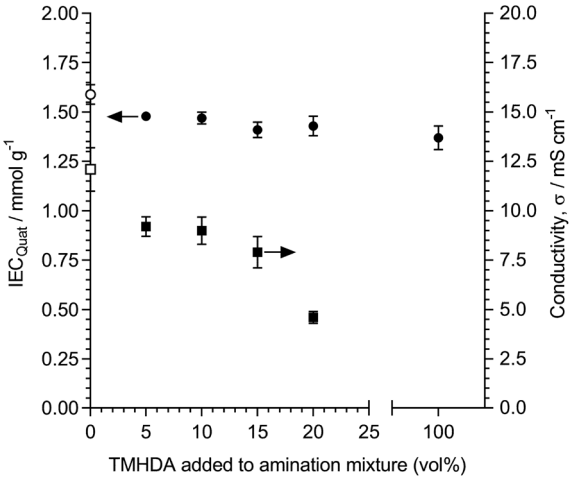


Fig. 10 The variation in IEC (circles) and $Cl^-$ conductivity (squares, in water, in-plane, 25 °C) of the RG-AEMs (MPIP) made using TMHDA in the amination stage. Error bars are sample standard deviations ($n = 3$).

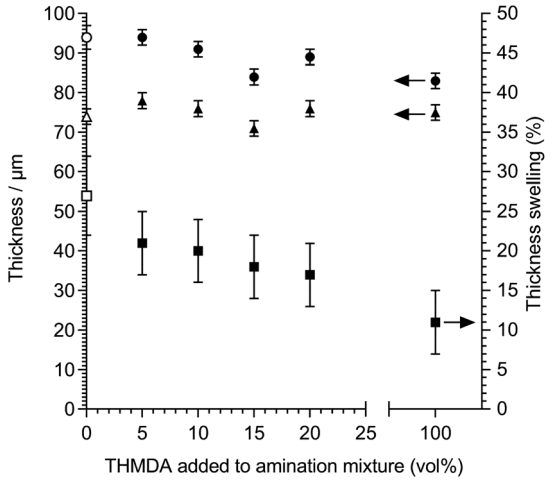


Fig. 12 The variation in hydrated thickness (circles), dry thickness (triangles) and dimensional swelling on hydration in the thickness direction (squares) of the RG-AEM (MPIP, $Cl^-$ forms) made using increasing TMHDA in the amination stage. Error bars for percentage thickness swelling values are propagated uncertainties calculated from the errors in measured thicknesses ($n = 3$ repeat measurements for each hydration state).

expected from the amount of TMHDA in the amination mixture. The most dramatic example of this is seen with EH-20 where nearly (40 ± 7) % of the $-CH_2Cl$ groups of the pre-aminated grafted membrane reacted with the TMHDA despite the amination mixture only containing 20 vol% TMHDA (which is equivalent to 22 mol% TMHDA-based – $NMe_2$ groups).

**Ion-exchange capacities, water uptakes and swelling.** Keystone properties for the EH-series of RG-AEMs are summarised in Table 2 (alongside data collected on Fujifilm commercial Type-10 AEM). The TMHDA-free EH-0 membrane (with MPIP-based head-group) had a slightly lower IEC compared to the DVB-free ED-0 membrane (with TMA-based head-group). The molar mass of the MPIP-based head-group is larger than the molar mass of the TMA-equivalent (99.17 g $mol^{-1}$ compared to 59.11 g $mol^{-1}$ for MPIP and TMA, respectively) so this naturally translates into slightly lower IECs.

With the use of TMHDA crosslinker, there is an added complication in that the diamine can react either at only one or both the terminal N atoms (Scheme 2). This can be probed by comparing $IEC_{Tot}$ to $IEC_{Quat}$ ($IEC_{Tot}$ is where the RG-AEMs were treated with aqueous HCl prior to titration to quaternise any residual, non-ionic tertiary amine groups). If $IEC_{Tot}/IEC_{Quat} = 1$ then this indicates that all of the reacted TMHDA molecules

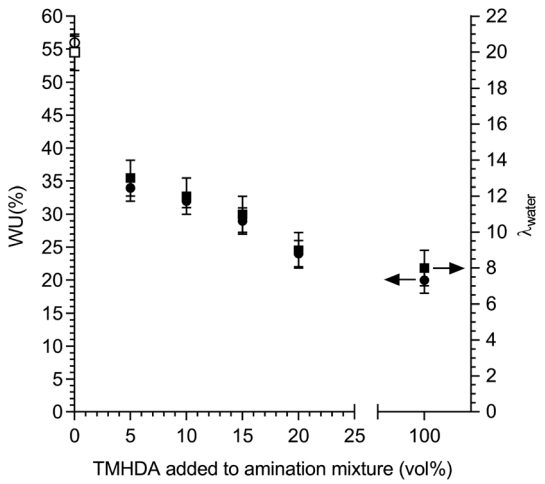


Fig. 11 The variation in gravimetric water uptake (WU, circles) and the number of $H_2O$ molecules per $Cl^-$ anion ($\lambda_{water}$, squares) of the RG-AEM (MPIP, $Cl^-$ forms) made using increasing TMHDA in the amination stage. Error bars for WU are sample standard deviations ($n = 3$). Error bars for $\lambda_{water}$ are propagated uncertainties calculated from the errors in measured IEC and WU values.

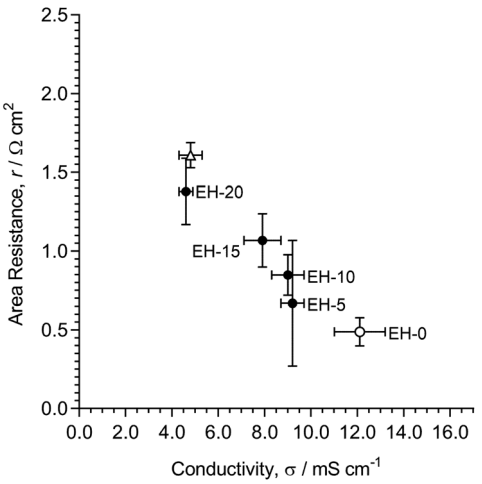


Fig. 13 The relationship between the room temperature (20–25 °C) through-plane area resistances (2-compartment cell containing aqueous NaCl (0.5 mol $dm^{-3}$) solution) and intrinsic $Cl^-$ conductivities (25 °C, in water, in-plane, no co-ions or excess counter-ions) of the RG-AEMs (MPIP) made using TMHDA crosslinker. The triangle datapoint is for the Fujifilm AEM (commercial benchmark).

have reacted with the $-CH_2Cl$ groups of the grafted poly(VBC) chains *via* both N atoms and are fully crosslinking in nature. If $IEC_{Tot}/IEC_{Quat} = 2$ then this indicates that all of the reacted TMHDA molecules have reacted with the $-CH_2Cl$ groups of the grafted poly(VBC) chains *via* only one N atom (fully non-crosslinking, as each covalently bound TMHDA-based head-group contains one unreacted tertiary amine). $IEC_{Tot}/IEC_{Quat}$ ratios between 1 and 2 indicate intermediate levels of crosslinking. The $IEC_{Tot}/IEC_{Quat}$ ratios for TH-5 to TH-100 are all <1.1 indicating that the incorporated TMHDA-based head-groups are predominantly crosslinking in nature. Hence, all further analysis will focus on the $IEC_{Quat}$ values.

As can be seen in Fig. 10, introduction of a small amount of TMHDA-crosslinking into the RG-AEMs (EH-5) resulted in a small drop in $IEC_{Quat}$ compared to the non-crosslinked EH-0, while a further increase in the amount of crosslinking (EH-10 to EH-20) does not lead to any further measurable drop in $IEC_{Quat}$ values. This is consistent with all TMHDA-based crosslinks being ionic, in contrast with DVB-based crosslinks that are non-ionic in nature; IEC will drop less dramatically on an increasing amount of TMHDA-crosslinking compared to DVB-crosslinking. The RG-AEM made using a pure TMHDA amination agent (EH-100, no MPIP during amination) had the lowest $IEC_{Quat}$ value recorded for the EH-*x* series (Table 2). EH-100 was also very brittle and hard to handle (without it mechanically breaking into small pieces – it was not possible to measure a conductivity) so this highly crosslinked RG-AEM is not practicable for use in large electrochemical cells.

As reported previously for ETFE-based non-crosslinked RG-AEMs, the WU for the MPIP-based variants are higher than for the TMA-based equivalents (*e.g.* EH-0 *vs.* ED-0 in Table 2).[10] The trend in changes of WU on increasing TMHDA-crosslinking is different to that seen with DVB-crosslinking. With the use of DVB (Fig. 5), initially the WU values decreased gradually on increasing levels of crosslinking with evidence of plateauing only seen at higher levels (ED-7.5 to ED-10). With the use of TMHDA (Fig. 11), the WU dropped dramatically between the non-crosslinked EH-0 and the lowest crosslinked version (EH-5)

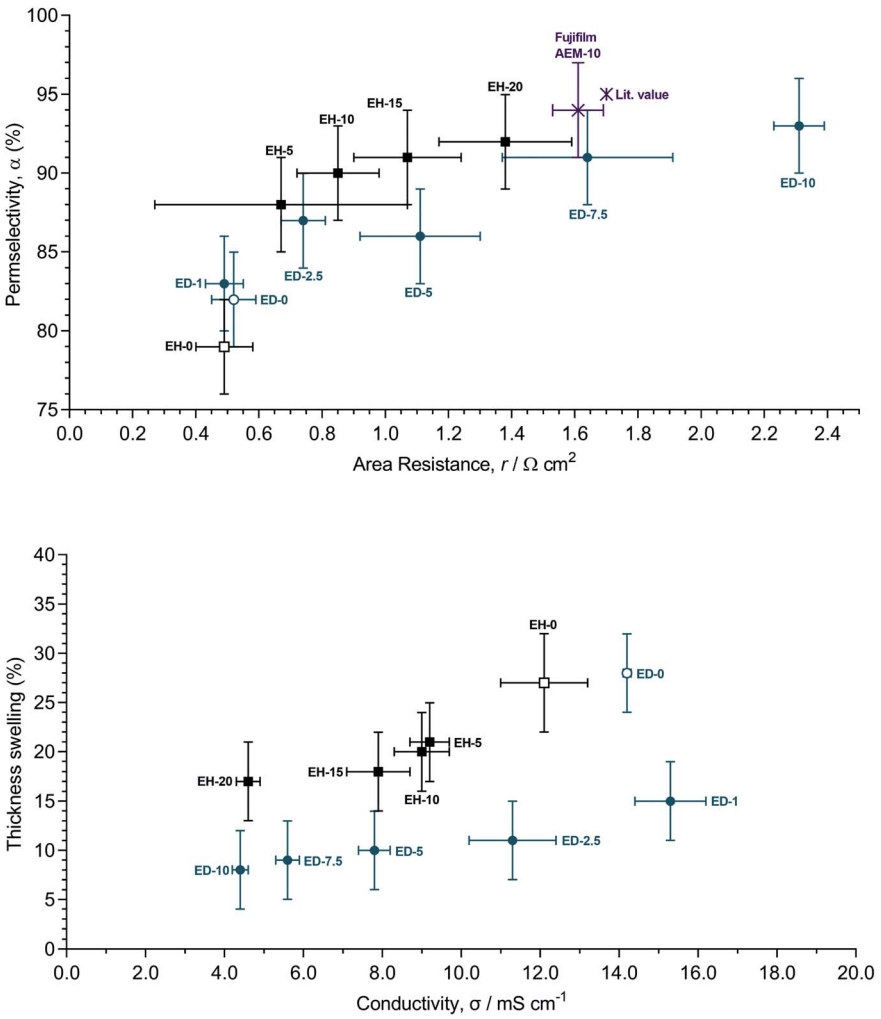


Fig. 14 A summary of the relationships between select properties for the RG-AEMs studied: (top) room temperature permselectivites *vs.* area resistances (in aqueous NaCl (0.5 mol $dm^{-3}$) solution); (bottom) room temperature thickness swelling *vs.* $Cl^-$ conductivities (in-plane, in water at 25 °C). Error bars are for repeat measurements on at least $n = 3$ samples of each RG-AEM (the error bars for the permselectivity were set at ±3% as this is the maximum uncertainty in the measurements, assuming a 1 mV uncertainty in potential measurements).

 

after which the rate of decrease in WU values declined on further introduction of additional crosslinking (EH-5 to EH-20). Even with full incorporation of ionic TMHDA-crosslinking (EH-100), the WU values did not drop significantly below 20% ($\lambda_{water} = 8 \pm 1$), (*cf.* higher levels of non-ionic DVB-crosslinking with WU = 15 ± 6% ($\lambda_{water} = 7 \pm 3$) for ED-10).

The thickness swelling also decreased with increasing amounts of TMHDA-crosslinking (Fig. 12). However, in contrast with the use of DVB-crosslinking, the drop in swelling when transitioning from the non-crosslinked EH-0 to lightly-crosslinked EH-5 was not as dramatic. Further crosslinking led to a gradual decrease in thickness swelling. Overall, the use of ionic TMHDA-crosslinking led to slightly higher levels of swelling (and WU) compared to the use non-ionic DVB-based crosslinking. Therefore, it is harder to restrict swelling using TMHDA as the crosslinker compared to the use of DVB. However, TMHDA (that produces ionic crosslinks) may have conductivity and resistance advantages.

**Ionic conductivity ($Cl^-$ form in water), area resistance (in contact with aqueous NaCl), and permselectivity.** As was observed with the use of DVB as a crosslinker, an increase in the level of TMHDA-crosslinking led to an increase in area resistance and a decrease in conductivity (Fig. 10 and 13). The drop in conductivity on increasing crosslinking levels showed a more complex pattern compared to the DVB-crosslinked versions. Despite dramatic drops in the intrinsic conductivities of the THMDA-crosslinked RG-AEMs, there was not such a negative effect on the application-relevant area resistance compared to the use of DVB-crosslinking (Fig. 13 *vs.* Fig. 7). An Increase in TMHDA-crosslinking led to increased $\alpha$ values (Table 2), with $\alpha$ >90% achievable without as much increase in area resistances compared to the use of DVB crosslinker.

## Summary and recommendation

Fig. 14 (bottom) summarises the relationship between the thickness swelling and $Cl^-$ conductivity for the radiation-grafted anion-exchange membranes (RG-AEMs) studied. Fig. 14 (top) summarises the relationship between permselectivity and area resistance, two application-critical properties for reverse electrodialysis (RED) cells. The use of a diamine crosslinker (*N*,*N*,*N*′,*N*′-tetramethylhexane-1,6-diamine, TMHDA, EH-5 to EH-20) in the amination step of RG-AEM fabrication has a less negative effect on resistance, and a more positive effect on permselectivity, compared to the use of divinylbenzene (DVB) crosslinker in the grafting step of RG-AEM fabrication (ED-1 to ED-10). The use of DVB-crosslinking, however, led to slightly better improvements (decreases) in thickness swelling compared to the use of TMHDA-crosslinking.

Overall, the use of TMHDA crosslinking gives the best balance between the RED application-relevant properties (permselectivity and area resistance). On a practical level, it is also the crosslinker that is easier to use. Therefore, for the development of crosslinked RG-AEMs for use in RED, where changes in dimensions between hydration states is less critical (as the AEMs are always submerged and fully hydrated), the use of TMHDA in the amination step is our recommended crosslinking method. However, considering the higher reductions in swelling achievable with DVB crosslinking, this type of crosslinking may well be more appropriate for other applications.

## Conflicts of interest

There are no conflicts to declare.

## Acknowledgements

This study is part of the REDAEM (Anion-Exchange Membranes for Reverse ElectroDialysis) project funded by the UK's Engineering and Physical Sciences Research Council (EPSRC grant EP/R044163/1). The Raman microscope was funded by EPSRC grant EP/M022749/1. Siân Franklin's PhD was funded by AFC Energy PLC (Dunsfold, Surrey). Terry Willson's PhD was funded on EPSRC grant EP/I004882/1. We thank Dr Friedrich Menges for granting us a free use licence to Spectragryph (https://www.effemm2.de/spectragryph/index.html).

## References

1 J. R. Varcoe, P. Atanassov, D. R. Dekel, A. M. Herring, M. A. Hickner, P. A. Kohl, A. R. Kucernak, W. E. Mustain, K. Nijmeijer, K. Scott, T. Xu and L. Zhuang, *Energy Environ. Sci.*, 2014, **7**, 3135.

2 J. Zhang, Y. He, K. Zhang, X. Liang, R. Bance-Soualhi, Y. Zhu, X. Ge, M. A. Shehzad, W. Yu, Z. Ge, L. Wu, J. R. Varcoe and T. Xu, *AIChE J.*, 2021, **67**, 17133; K. Yassin, I. G. Rasin, S. Brandon and D. R. Dekel, *J. Membr. Sci.*, 2020, **608**, 118206; B. Achrai, Y. Zhao, T. Wang, G. Tamir, R. Abbasi, B. P. Setzler, M. Page, Y. Yan and S. Gottesfeld, *J. Electrochem. Soc.*, 2020, **167**, 134518; X. Peng, D. Kulkarni, Y. Huang, T. J. Omasta, B. Ng, Y. Zheng, L. Wang, J. M. LaManna, D. S. Hussey, J. R. Varcoe, I. V. Zenyuk and W. E. Mustain, *Nat. Commun.*, 2020, **11**, 3561; Y. S. Kim, *ACS Appl. Polym. Mater.*, 2021, **3**, 1250; M. Mandal, G. Huang, N. Ul Hassan, W. E. Mustain and P. A. Kohl, *J. Mater. Chem. A*, 2020, **8**, 17568; J. Wang, Y. Zhao, B. P. Setzler, S. Rojas-Carbonell, C. B. Yehuda, A. Amel, M. Page, L. Wang, K. Hu, L. Shi, S. Gottesfeld, B. Xu and Y. Yan, *Nat. Energy*, 2019, **4**, 392; S. Gottesfeld, D. R. Dekel, M. Page, C. Bae, Y. Yan, P. Zelenay and Y. S. Kim, *J. Power Sources*, 2018, **375**, 170; J. Ran, L. Ding, C. Chu, X. Liang, T. Pan, D. Yu and T. Xu, *J. Mater. Chem. A*, 2018, **6**, 17101.

3 D. Henkensmeier, M. Najibah, C. Harms, J. Žitka, J. Hnát and K. Bouzek, *J. Electrochem. Energy Convers. Storage*, 2021, **18**, 024001; H. A. Miller, K. Bouzek, J. Hnat, S. Loos, C. I. Bernäcker, T. Weißgärber, L. Röntzsch and J. Meier-Haack, *Sustainable Energy Fuels*, 2020, **4**, 2114; P. Fortin, T. Khoza, X. Cao, S. Y. Martinsen, A. O. Barnett and S. Holdcroft, *J. Power Sources*, 2020, **451**, 227814; R. Abbasi, B. P. Setzler, S. Lin, J. Wang, Y. Zhao, H. Xu, B. Pivovar, B. Tian, X. Chen, G. Wu and Y. Yan, *Adv. Mater.*, 2019, **31**, 1805876.

4 D. A. Salvatore, C. M. Gabardo, A. Reyes, C. P. O'Brien, S. Holdcroft, P. Pintauro, B. Bahar, M. Hickner, C. Bae, D. Sinton, E. H. Sargent and C. P. Berlinguette, *Nat. Energy*,

2021, **6**, 339; B. Endrődi, E. Kecsenovity, A. Samu, T. Halmágyi, S. Rojas-Carbonell, L. Wang, Y. Yan and C. Janáky, *Energy Environ. Sci.*, 2020, **13**, 4098; M. Ma, E. L. Clarke, K. T. Therkildsen, S. Dalsgaard, I. Chorkendorff and B. Seger, *Energy Environ. Sci.*, 2020, **13**, 977; Z. Yin, H. Peng, X. Wei, H. Zhou, J. Gong, M. Hai, L. Xiao, G. Wang, J. Lu and L. Zhuang, *Energy Environ. Sci.*, 2019, **12**, 2455.

5 L. Zeng, T. S. Zhao, L. Wei, H. R. Jiang and M. C. Wu, *Appl. Energy*, 2019, **233–234**, 622; M. Abdiani, E. Abouzari-Loft, T. M. Ting, P. M. Nia, S. S. Sha'rani, A. Shockravi and A. Ahmad, *J. Power Sources*, 2019, **424**, 245.

6 J. Jang, Y. Kang, J.-H. Han, K. Jang, C.-M. Kim and I. S. Kim, *Desalination*, 2020, **491**, 114540; H. Tan, Y. Wang, Y. Pei and J. C. Crittenden, *Appl. Energy*, 2020, **262**, 114482; C. Capparelli, C. R. Fernandez Pulido, R. A. Weincek and M. A. Hickner, *ACS Appl. Mater. Interfaces*, 2019, **11**, 26298; Y. J. Lee, M. S. Cha, S.-G. Oh, S. So, T.-H. Kim, W. S. Ryoo, Y. T. Hong and J. Y. Lee, *RSC Adv.*, 2019, **9**, 27500; R. A. Tufa, S. Pawlowski, J. Veerman, K. Bouzek, E. Fontananova, G. di Profio, S. Velizarov, J. G. Crespo, K. Nijmeijer and E. Curcio, *Appl. Energy*, 2018, **225**, 290; D. H. Cho, K. H. Lee, Y. M. Kim, S. H. Park, W. H. Lee, S. M. Lee and Y. M. Lee, *Chem. Commun.*, 2017, **53**, 2323; B. E. Logan and M. Elimelech, *Nature*, 2012, **488**, 313.

7 J. Liao, H. Ruan, X. Gao, Q. Chen and J. Shen, *J. Membr. Sci.*, 2021, **621**, 118999; S. Pal, R. Mondal, S. Guha, U. Chatterjee and S. K. Jewrajka, *J. Membr. Sci.*, 2020, **612**, 118459.

8 J. Pan, B. Wei, H. Xie, J. Feng, S. Liao, X. Li and Y. Yu, *Sep. Purif. Technol.*, 2021, **265**, 118526; M. M. Alam, M. Hossain, Y. Mei, C. Jiang, Y. Wang, C. Y. Tang and T. Xu, *Desalination*, 2021, **497**, 114779.

9 M. M. A. Mahmoud, K. Yoshimura and Y. Maekawa, *J. Membr. Sci.*, 2021, **620**, 118844; J. C. Douglin, J. R. Varcoe and D. R. Dekel, *Journal of Power Sources Advances*, 2020, **5**, 100023; A. Zhegur-Khais, F. Kubannek, U. Krewer and D. R. Dekel, *J. Membr. Sci.*, 2020, **612**, 118461; R. Espiritu, B. T. Golding, K. Scott and M. Mamlouk, *J. Mater. Chem. A*, 2017, **5**, 1248; T. P. Pandey, A. M. Maes, H. N. Sarode, B. D Peters, S. Lavinia, K. Vezzu, Y. Yang, S. Poynton, J. R. Varcoe, S. Seifert, M. Liberatore, V. Di Noto and A. Herring, *Phys. Chem. Chem. Phys.*, 2015, **17**, 4367; M. Mamlouk, J. A. Horsfall, C. Williams and K. Scott, *Int. J. Hydrogen Energy*, 2012, **37**, 11912; J. Fang, Y. Yang, X. Lu, M. Ye, W. Li and Y. Zhang, *Int. J. Hydrogen Energy*, 2012, **37**, 594; T. N. Danks, R. C. T. Slade and J. R Varcoe, *J. Mater. Chem.*, 2002, **12**, 3371.

10 J. Ponce-Gonzalez, D. K. Whelligan, L. Wang, R. Bance-Soualhi, Y. Wang, Y. Peng, H. Peng, D. C. Apperley, H. N. Sarode, T. P. Pandey, A. G. Divekar, S. Seifert, A. M. Herring, L. Zhuang and J. R. Varcoe, *Energy Environ. Sci.*, 2016, **9**, 3724.

11 T. R. Willson, I. Hamerton, J. R. Varcoe and R. Bance-Soualhi, *Sustainable Energy Fuels*, 2019, **3**, 1682.

12 Y. Ji, H. Luo and G. M. Geise, *Phys. Chem. Chem. Phys.*, 2020, **22**, 7283.

13 G. M. Geise, M. A. Hickner and B. E. Logan, *ACS Appl. Mater. Interfaces*, 2013, **5**, 10294.

14 L. Wang and M. A. Hickner, *Polym. Chem.*, 2014, **5**, 2928.

15 S. Holmberg, J. H. Näsman and F. Sundholm, *Polym. Adv. Technol.*, 1996, **9**, 121.

16 E. N. Komkova, D. F. Stamatialis, H. Strathman and M. Wessling, *J. Membr. Sci.*, 2004, **244**, 25.

17 H. Fan and N. Y. Yip, *J. Membr. Sci.*, 2019, **573**, 668.

18 L. Wang, E. Magglioccа, E. L. Cunningham, W. E. Mustain, S. D. Poynton, R. Escudero-Cid, M. M. Nasef, J. Ponce-Gonzalez, R. Bance-Souahli, R. C. T. Slade, D. K. Whelligan and J. R. Varcoe, *Green Chem.*, 2017, **19**, 831.

19 L. Wang, X. Peng, W. E. Mustain and J. R. Varcoe, *Energy Environ. Sci.*, 2019, **12**, 1575; L. Wang, M. Bellini, H. A. Miller and J. R. Varcoe, *J. Mater. Chem. A*, 2018, **6**, 15404; L. Wang, J. J. Brink, Y. Liu, A. M. Herring, J. Ponce-Gonzalez, D. K. Whelligan and J. R. Varcoe, *Energy Environ. Sci.*, 2017, **10**, 2154.

20 W. Chen, M. Mandal, G. Huang, X. Wu, G. He and P. A. Kohl, *ACS Appl. Energy Mater.*, 2019, **2**, 2458.

21 W. Luo, L. Wang, R. Feng, C. Zhao, J. Wang and T. Cai, *J. Appl. Polym. Sci.*, 2020, **138**, 49872.

22 P. Długołęcki, K. Nymeijer, S. Metz and M. Wessling, *J. Membr. Sci.*, 2008, **319**, 214.

23 J. G. Hong and T. W. Park, *J. Electroanal. Chem.*, 2018, **818**, 134.

24 T. Sata, *J. Membr. Sci.*, 2000, **167**, 1.

25 G. M. Geise, L. P. Falcon, B. D. Freeman and D. R. Paul, *J. Membr. Sci.*, 2012, **423**, 195.

26 A. R. Khare and N. A. Peppas, *Biomaterials*, 1995, **16**, 559.

27 P. Długołęcki, P. Ogonowski, S. J. Metz, M. Saakes, K. Nijmeijer and M. Wessling, *J. Membr. Sci.*, 2010, **349**, 369.

28 A. L. Gonçalves Biancolli, D. Herranz, L. Wang, G. Stehlíková, R. Bance-Soualhi, J. Ponce-González, P. Ocón, E. A. Ticianelli, D. K. Whelligan, J. R. Varcoe and E. I. Santiago, *J. Mater. Chem. A*, 2018, **6**, 24330.

 